Photo-Initiated Chemical Vapor Deposition of Thin Films using Syngas for the Functionalization of Surfaces at Room Temperature and Near-Atmospheric Pressure

C.A.Dorval Dion, W.Raphael, E.Tong, J.R.Tavares*

Department of Chemical Engineering, École Polytechnique de Montréal, C.P. 6079, Succ. Centre-Ville, Montreal, Quebec, Canada, H3C 3A7

Abstract

Hydrophilic and hydrophobic thin films have been deposited onto flat metallic substrates through photo-initiated chemical vapour deposition (PICVD), using syngas a as precursor, and affordable UVC germicidal lamps as a source of light. This study is the first experimental investigation of what has been previously concluded to be the potential solution to the current widespread nanoparticle functionalization problem. This study addresses the current limiting factor, namely the cost issue, by using simple gas precursors, using an affordable initiation source and operating under normal condition. This approach differs from the current approaches which use expensive solvents as precursors, energy consuming-sources of initiation (e.g. high temperature, plasma and VUV) and operate under high vacuum and/or high temperatures. While the current paradigm is to target the peak absorption of a molecule, the present study indicates that long chain polymerized products can be formed from off-peak wavelength. It has been found that photo-initiated deposition occurs and that a wide range of water contact angles, from 5° to 118°, can be obtained by manipulating the experimental conditions. A multilinear empirical model has been derived, and it predicts fairly well the contact angles obtained as a function of the different experimental parameters.

Keywords: PICVD, Syngas, UV, Photopolymerization, Surface functionalization, Thin film

Nomenclature

CVD Chemical vapour deposition

$iCVD$ Initiated chemical vapour deposition

P Reactor pressure

$PECVD$ Plasma-enhanced chemical vapour deposition

*Corresponding author: jason.tavares@polymtl.ca

$PICVD$ Photo-induced or -initiated chemical vapour deposition

Pos Position in the reactor

r H_2/CO gas ratio

$TACVD$ Thermally-activated chemical vapour deposition

x Water contact angle

1. Introduction

Due to their high surface/volume ratio, nanoparticles exhibits interesting properties that promise a brillant future for many applications such as adsorption, absorption and heat transfer [1]. However, even if nanoparticles have mobilized the attention of scientists, they are still not adopted industrially as much as they could be. Among the reasons behind this is the fact that particle agglomeration issues remain an important practical limitation. Typical approaches to counter this problem are through the use of surfactant. While the use of surfactants possesses numerous advantages (cost, simplicity, efficiency), these compounds are simply adsorbed to the surface and not chemically attached to it. Weak adsorption bonds imply that surfactants can detach from the surface when heated above temperatures as low as 70°C [2]. While this solution has allowed the use of nanoparticles for a limited range of room-temperature applications, a new solution is still required for high-temperature applications such as nanofluids, nanocomposite preparation, etc. This new solution would benefit from being based on a strong covalent bond between the functional compound and the particle, instead of simply counting on weak physical adsorption. Also, nanoparticle manufacturing already being a costly process, to make sure of its adoption, a functionalization technology must not only be reliable but also affordable and scalable.

Surface functionalization through chemical vapour deposition (CVD) shows great promises as a potential solution. The advantages of gas phase methods are considerable: these processes are considered as cleaner and simpler as they do not involve liquids. Dry processes also simplify downstream separation. CVD is also recognized as a method that is capable of producing dense and pure materials on complex shapes. Another advantage of the gas phase method is that it can be operated as a continuous process instead of a batch process. This can have a tremendous effect on the profitability of an industrial scale system [3]. Different variations of the chemical vapour deposition technique exists, such as thermally activated-, plasma enhanced- and photo initiated- chemical vapour deposition (respectively TACVD, PECVD and PICVD), and each of them has strengths and weaknesses. Our research group previously concluded that PICVD showed potential for large scale gas phase treatment for the surface functionalization of nanoparticles at normal conditions and low cost [4]. Since large scale nanoparticle synthesis is usually accomplished in the

gas phase, it would make sense if the subsequent functionalization process was also a gas phase process. We thus present an experimental proof of concept of PICVD for surface functionalization on flat substrates.

2. Theoretical Framework

2.1. Chemical Vapor Deposition Theory

The fundamental aspects of CVD will not be reviewed in depth here, since this has been done thoroughly already [5, 6, 7]. Also, the different forms of CVD applicable to the current situation have already been reviewed and compared in our previous paper [4].

Baxamusa *et al.* have previously reported that PICVD was able to produce thin films (100 nm) near room temperature under unspecified "mild" vacuum conditions. They also indicated that the technique would be suitable for coating particles having diameters as small as 5 microns [8]. However, nothing indicates that it could not be done with finer particles. They reported that PICVD was a more "gentle" method than PECVD, which explains their choice to go with PICVD for the coating of sensitive sensors such as protein detectors. Due to a slower deposition rate as well as the presence of UV light, the curing is achieved by default during the whole operation. This explains why PICVD is able to produce such crosslinked structures. Baxamusa *et al.* reported to be even able to "tune" the crosslink density, which means that the mechanical properties of the film could be tailored.

PICVD typically refers to systems using vacuum ultraviolet (VUV), which is low wavelength/high energy UV light. It is important to mention that the cost is very high in that situation, namely for two reasons: first, the system has to operate under high vacuum because the radiation is intensely absorded by gases and secondly, the reactor window, in order to let these wavelengths pass through must be made of highly expensive exotic materials such as MgF_2, LiF or CaF_2.

Most of the work done with PICVD has targeted acrylates precursors, mainly because of their high photosensitivity. Those compounds are usually liquid at ambiant conditions, and thus operation under low pressure or heating to vaporize small amounts becomes a prerequisite; using gas precursors is a way to curtail this requirement. To polymerize from gases, it is usually required to have both a polymerization backbone (a source of carbon) and a source of hydrogen to saturate the carbon atom to the needed degree. Carbon sources in the gas domain tend to be very small for obvious reasons, such as CH_4, C_2H_6, C_3H_8. Zhang et al. [9] used short-chain hydrocarbons, mainly alkanes. For the present study, the objective being to introduce functionality to the surface, there is a need of oxygen in the reactor. Knowing that CO and H_2 is a common gas combination resulting from gasification processes, this gas mixture seemed pertinent. Additional reasons making CO and H_2 an interesting choice:

- Having two gases instead of one opens up the possibility to produce a wide range of different products. Different kinetics and stoichiometry should result in different compounds.

- CO and H_2 being a mix of gases often present together in industry (e.g. products of the gasification process), it could be very convenient to use those products as process inlets.
- Fischer-Tropsch synthesis (FTS) is a similar reaction that consists to reconstruct long chains of carbon from syngas. First, it proves that the reaction is feasible thermodynamically, and second, knowledge gaps can be filled by borrowing information from those researches. Tavasoli *et al.* has already enhanced FTS with UV light [10].
- Finally, the CO bonds are known to produce radicals under UV light [11]. The gas mixture could thus react without the need for a photoinitiator or photosensitizer.

The bond dissociation energies of CO and H_2 are respectively 11.09 eV and 4.478 eV. Since the main wavelength emitted by the UVC lamp is 254 nm, which corresponds to 4.88 eV, even at complete absorption only the hydrogen would be dissociated. However, it is worth mentioning that the radiation can nevertheless open constituent π bonds, thus electronically exciting the CO molecule and therefore contributing to the kinetic enhancement of the reaction. Further, it is known that carbonyl species tend to decompose into radicals under UV light below 267 nm [8], which is close to the CO configuration. It is worth mentioning that standard 254 nm germicidal lamps also have an emission peak around 185 nm.

Scott *et al.* have previously shown that 254 nm germicidal lamps were effective in eliminating gaseous contaminants such as carbon monoxide and VOCs [12]. They discussed the importance of the ratio 185 nm versus 254 nm necessary to eliminate low concentration of CO in gas stream. Commercially available low-pressure mercury-vapor lamps emit about 86% of their light at 254 nm, the rest being mainly attributed to 185 nm. Although 185 nm may provide more energy, the quartz glass used in commercially available lamps are more opaque to 185 nm than 254 nm [13].

2.2. The photochemistry of syngas

Although several articles have studied the photochemistry of carbon monoxide and hydrogen independently, there is very little about the photochemistry syngas as a mixture. This could be explained by the fact that the synthesis gas is a relatively new concept, which is gaining interest with the development of gasification technology. Finally, another more practical explanation could be that at first glance, the theory does not suggest that these two gases could react together when subjected to low energy lamps.

Hydrogen by itself has little interest in photochemistry, due to the limited amount combinations of reactions possible. The hydrogen molecule requires an energy of 4.478 eV and thus theoretically could be dissociated by a 254 nm lamp. However, hydrogen absorbs light in a very narrow range of wavelength, between 85 and 110 nm .

In the same vein, any formation of photochemical products from carbon monoxide using a lamp exceeding 111 nm wavelength, if any, would necessarily be due to the formation of radicals [11], since the energy required

to dissociate the molecule is 11.09 eV[1]. This electronically excited state ($a^3\pi$), however can produce reactions that otherwise would not occur. For example, CO is known to produce the C_3O_2 in the presence of krypton (605 nm) and xenon (185 nm) lamps, which theoretically do not possess the required energy. The reaction products of CO $a^4\pi$ is the CO_2 and C_3O_2 [11]. The proposed mechanism is the following [14]:

$$CO \overset{hv}{\rightarrow} CO* \tag{1}$$

$$CO* + CO \rightarrow CO_2 + C \tag{2}$$

$$C + CO \rightarrow C_2O \tag{3}$$

$$C_2O + CO \rightarrow C_3O_2 \tag{4}$$

It is worth noting that the last two steps of the mechanisms recall the behavior of a cationic polymerization [15]:

$$M^+ + M \rightarrow MM^+ \tag{5}$$

$$MM^+ + nM \rightarrow M[M_n]M^+ \tag{6}$$

Which would imply that the growth of the product could be summarized in the following manner where applicable:

$$C_nO_{n-1} + CO \rightarrow C_{n+1}O_n \tag{7}$$

It is quite possible that some steps of the mechanisms presented above are transferable to the photochemical synthesis gas. For example, given the presence of hydrogen, it would be tempting to think that the oxygen with the free electron pair could react with hydrogen to form water, which is a very stable product. The reaction could then continue its course as before.

$$CO \overset{hv}{\rightarrow} CO* \tag{8}$$

$$CO* + H_2 \rightarrow C^+ + H_2O \tag{9}$$

$$C + CO \rightarrow C_2O \tag{10}$$

$$C_2O + CO \rightarrow C_3O_2 \tag{11}$$

Another potential effect of the presence of hydrogen could be that the carbons of the chain would tend to saturate. This suggests that a photochemical reaction involving the synthesis gas has the potential to carry large molecules of the form $C_xH_yO_z$ as well as water (H_2O). This could promote the production of OH groups, which are generally desired in the treatment of a hydrophilic surface.

[1] which corresponds to about 111 nm to 100 % absorption

2.3. Similarities with the Fischer-Tropsch synthesis

Since the objective is to generate long-chain compounds of carbon from synthesis gas, it is difficult to avoid the comparison with the Fischer-Tropsch synthesis. The Fischer-Tropsch synthesis has been developed in Germany during the first world war, seeking to produce diesel from synthesis gas. Even today, this reaction is of interest for research because it is an alternative to fossil fuels.

The Fischer-Tropsch reaction can be expressed in the following general manner:

$$(2n+1)H_2 + nCO \rightarrow C_nH_{2n+2} + nH_2O \tag{12}$$

This reaction is exothermic and requires a catalyst in order to reduce the activation energy necessary for it to take place. The generally accepted reaction mechanism, where S is an anchor point on the surface is [16]:

$$CO + 2S \rightarrow C \cdot S + O \cdot S \tag{13}$$

$$C \cdot S + H_2 \rightarrow CH_2 \cdot S \tag{14}$$

$$2(C \cdot S) + 3H_2 \rightarrow 2(CH_3 \cdot S) \tag{15}$$

$$R - CH_2 \cdot S + CH_2 \cdot S \rightarrow R - CH_2 - CH_2 \cdot S + S \tag{16}$$

$$R - CH_2 - CH_2 \cdot S \rightarrow R - CH = CH_2 + S \tag{17}$$

$$2(R - CH_2 - CH_2 \cdot S) + H_2 \rightarrow 2(R - CH2 - CH_3) + 2S \tag{18}$$

As mentioned previously, that Tavasoli *et al.* investigated the Fischer-Tropsch reaction in the presence of a UV lamp. The group reported that the presence of light had more than quadrupled the apparent catalyst activity compared to control tests without light. The group also reported a difference with the control tests in terms of product selectivity. Indeed, the presence of light seemed to move selectivity towards products lengths C_5 et C_{11}, over C_{12+} [10].

Although the group uses the term "photocatalysis", it is important to note that these experiments were conducted in the presence of solid catalysts in both cases (with and without light). Solid catalysts used were all cobalt-based, but the supports were varied. The support materials tested were alumina (Al_2O_3), silica (SiO_2), and titanium dioxide(TiO_2). The authors concluded that catalysts supported by titania were more sensitive to light, leading to significant improvements in terms of activity.

This last statement leads naturally to question as to whether or not the presence of metals in a reactor PICVD could act as a catalyst. Under the current research project, it is intended to use copper substrates in order to prove the concept of PICVD applied to surface treatment. Although copper is not considered a Fischer-Tropsch catalyst, studies have tested the effect of copper as a promoter in Fischer-Tropsch catalysts. The researchers came to the conclusion that not only the addition of copper improves the overall performance, but would also tend to favor the production of alkenes versus that of alkanes [17]. These findings may

foreshadow the fact that a Fischer-Tropsch reaction, both photo-assisted and in the presence of copper, has the potential to yield to outstanding results.

2.4. Reactions of a PICVD process

Baxamusa *et al.* proposed a reaction mechanism for PICVD, based on the hypothesis that reactions are initiated by radicals [8]. The first step shows that the light decomposes the organic monomer radicals. The authors state that this step can be completed either in the gas phase or once the gas is adsorbed on the surface. In both cases, the radicals on the surface react with absorbed monomers to grow polymerized products. In this case, the study does not mention any gas phase reaction other than the formation of radicals and thus implies that the PICVD reaction would require an active site onto the surface in order to catalyze the reaction.

It is also known that the radicals might be the driving force of cyclization [18], which indicates that the presence of rings in the PICVD products was not surprising.

Finally, Andrzejewska [19] explains that deposits produced by photoinitiators offer a very high degree of crosslinking. Still due to the presence of free radicals, the propagation continues through three (3) different pathways, namely:

1. The addition of another monomer.
2. The addition of an adjacent complex molecule (intermolecular crosslinking).
3. A cyclization reaction (intramolecular crosslinking).

All this leads to the formation of a complex highly interconnected network. Figure 1 illustrates the words described above.

[Figure 1 about here.]

2.5. Mass transfer phenomena

It is difficult to talk about gas-solid reaction systems without mentioning the effects of mass transfer phenomena. By definition, the CVD method is a surface reaction. The reaction rate is not only based on the intrinsic kinetics, but on all the steps leading to the reaction, including the internal and external mass transfer. In other words, before reacting to the surface, the molecules must first reach the active site. Although this concept may seem simple in theory, mass transfer is often the limiting step in surface reactions. This can also lead to several practical problems in the case of CVD [20, 21]. For example, if the surface functionalization of nanoparticles is to be carried out in a fluidized bed, the theory says that the superficial velocity should be increased to counter the effects of external mass transfer [22]. However, this may cause particle entrainment by the gas stream. Also dependently of their geometry and porosity, nanoparticles could also be subject to phenomena of internal mass transfer. The main parameters influencing the mass transfers in a reactor according Choy [7] are listed below.

1. Mean temperature and temperature profiles in the reactor
2. Reactor pressure
3. Gas flow rate
4. Gas properties
5. Reactor geometry

The latter is very critical since it can cause flow patterns that may affect several aspects, including the uniformity of a photochemical deposition.

3. Methodology

3.1. Materials

Copper substrates were multipurpose copper (Alloy 110) sheets supplied by McMaster-Carr trimmed to 1.5 cm by 1 cm coupons. Argon (HP+), CO (Pur T-44) and H_2 (UHP T-30) were supplied by Air Liquide. The reactor was made of two custom built 45 cm long quartz tubes with standard 24/40 taper joints and supplied by Technical Glass Products. All experiments were conducted with a dual-bulb 254 nm UVC germicidal lamps of 96 cm in length supplied by Cole-Parmer which offers 5.5×10^{-4} W/cm^2 of light intensity. The light intensity was measured with an International Light Technologies ILT 1700 Research Radiometer. The joints were sealed using standard clips and high vacuum laboratory grease (Dow Corning). The massflow controller were part of the 5850E Brooks series and calibrated for each gas. The sandpaper used for substrate polishing was 2500 grit supplied by McMaster-Carr.

3.2. Experiment

The experimental setup is shown in figure 2. The gas mixture is fed to custom made quartz tube, where the gas is to be irradiated by the UV lamp. The flat copper substrates to be treated were placed into the reactor onto a custom made holder having a capacity of 5 coupons. The H_2 and CO gas ratio was controlled by adjusting each gas individual massflow controller. The experiment duration was fixed to 1 hour. Before any experiments, the copper coupons were thouroughly polished using deionized water and sandpaper. An 18 cm long and 1.5 cm wide holder was used to insert the freshly polished substrates into the reactor. A total of 5 copper substrates, spaced 3.5 cm apart, could be inserted at the same time. The coupon were inclined with an angle of 45° with respect to the gas flow.

[Figure 2 about here.]

Copper was used because it has been known to work with PECVD [23], so a comparative standard exists. The temperature inside the reactor was monitored with an IR temperature sensor with an emissivity factor of 0.75. The operating pressure in the reactor was controlled via a 3-way valve placed at the output. One of the two outputs of the valve was linked to a vacuum line, while the second was leading to a fume hood. This

configuration allowed a pressure range from +/- 10 kPa gauge. The quartz tubes were previously cleaned by submerging them in a solution of NaOH 5.0M for 24 hours. They were then rinsed with distilled water and air dried. Before any experiments, argon was used to purge the reactor for 3 minutes. The reactor was then covered with standard commercial aluminium foil. When the experiments were completed, the copper substrates were carefully taken out of the reactor and placed in a plastic container filled with argon.

Experimental conditions. The effects of the following parameters have been tested:

- H_2/CO molar ratio (varying from 1/16 to 4),
- Total flow rates (varying from 260 to 1000 mL/min),
- Position in the reactor from 1 to 8 (8 arbitrary positions uniformly spaced apart from each other in the second tube, spacing being 1/8 of the tube length)
- Pressure in the reactor (varying from -10 to +10 kPa gauge),
- Delay before analysis (in number of days after deposition of the coating),
- Order of experiment (to identify and control for cumulative effects over time, for example lamp degradation)
- Light intensity (increased by partially or totally enclosing the lamp together with the reactor using aluminium paper). Note: this also has the effect of increasing the reactor temperature as well by about 30°C.

A secondary objective was to test the capacity of H_2O_2 to act as a photoinitiator because of its absorption peak that falls directly onto the 254 nm wavelength, which corresponds exactly to the lamp emission. For these experiments, 0 to 10 mL/h was injected in to the reactor by the mean of a peristaltic pump. H_2O_2 used was 50% concentrated and supplied by Fischer Scientific.

3.3. Modeling methodology

Design of experiment and multivariate analysis. As the present study represents an investigation of a wholly new process, experimental design was applied to determine the effect of a large variety of parameters and trends were extracted through a multivariate analysis. The first step of this method consists in normalizing the data, as well as the response (here being the resulting contact angle). Once normalized, it becomes fairly easy to derive emperical models, usually starting by trying multilinear regression, then increasing the complexity if needed. Having three levels (-, 0, +) per parameters helps to determine either if the relationship between the parameter and the response is linear or better approximated by a polynomial. Also, sometimes some parameters by themselves do not have effect, but do have an effect when combined with another factor.

The modeling was achieved following a multilinear approach using the Microsoft Excel solver to find the parameter coefficients. The approach consisted of trying to model with parameters individually, and then trying combined effects.

3.4. Characterization

The treated copper substrates were analyzed by goniometry with distilled water, Fourier transform infrared spectroscopy (FTIR) (Spectrum 65 from Perkin Elmer) and field emission scanning electron microscopy (FESEM) (JEOL JSM7600F). The exiting gases were captured through an acetone bubbling column (A18P-4, Fischer Scientific) for analysis by GCMS. The acetone was Chromasolv for HPLC grade ($\geq$ 99.9 % purity) and supplied by Sigma Aldrich. The GCMS system was a Agilent 7890A matched with a HP-88 column matteched with the quadrupole Agilent 5975 detector operated at a helium flow rate of 1.5 mL/min. The light intensity was monitored by a Ocean Optics USB2000 spectrophotometer. The goniometry measurements were achieved by placing 4 μL of distilled water on every copper samples. The sessile drop water contact angle being stable on the minute time frame, one measurement per location was taken immediately for 5 locations per sample using a NRL C.A. Goniometer (Model No. 100-00 115). Figure 3 represents a typical sample and shows the 5 locations where measurement were taken.

[Figure 3 about here.]

4. Results

The results showed that, indeed, PICVD was able to functionalize the surface of copper substrate using syngas as precursor. Figure 4 demonstrates the before and after effect of such coating.

[Figure 4 about here.]

4.1. Modeling results

The modeling of the PICVD process has been made in two steps. The first one being an overall mapping of the conditions and process parameters, while the second one was a refinement of the first one. This approach helped to eliminate the non-significant parameters and, at the same time, gave indication about what direction to go in order to push the boundaries, and therefore expand the validity of the model. As a result, the model's coefficient readjusted a little, and some parameters, like the delay before analysis, could be excluded simply by adapting the procedure.

Looking at some visible coatings that were obtained (bottom picture, figure 4), it can be noticed that surface coverage is non-uniform, therefore measuring the contact angle of very thin or non-existant coating instead of the evident "sweet spot". Since the objective is to model the contact angle of the coating, and not the surface in average, the data must be filtered accordingly. The measurement procedure can be easily readjusted when the coating is visible, but data filtering can be more complicated when the coating is

invisible, which was the case most of the time. First, the measurement corresponding to the copper's native water contact angle ($\bar{x}_{copper}$=70°) were dismissed right away. Futhermore, figure 5 shows that the coating usually has a fade with multiple shade of colors, and indeed the contact angles varied accordingly.

[Figure 5 about here.]

Tables 1 to 3 presents the parameters for the series of experiment conducted during 1 hour, including the water contact angle measured as well as some additional information. The "selected" column represents the angle considered for the model for a specific experiment. The selection was made according to equation 19. This selection prior to modelling was necessary due to the lack of uniformity noted on the surfaces. Since the contact angle of the copper is known, it was possible to determine where the coating was present by picking the measurement that was the furthest from the copper, no matter what direction (hydrophilic or hydrophobic). In other words, this study was more concerned about the difference than the absolute contact angle. These experiments have allowed for reaching contact angles from 30° to 100°, without the addition of photoinitiator or sensitizers, simply by mapping the experimental conditions. More extreme values have been obtained when using H_2O_2 and running for extended periods (up to 3 hours).

[Table 1 about here.]

[Table 2 about here.]

[Table 3 about here.]

$$x_{selected} = x\left(\underset{\text{i = 1 to 5}}{\arg\max}|x_i - \bar{x}_{copper}|\right) \tag{19}$$

This lack of uniformity can be due to the flow dynamics of the system. As a first proof of concept, the emphasis was on the most extreme value, assuming that uniformity is an issue that can be addressed subsequently. In other words, this study focused on what was achievable rather than on an average uniformity-biased efficiency. The following empirical model has been derived from the data for the experiment without hydrogen peroxide (experiments presented in table 1):

$$x_{selected}(^\circ) = A \cdot P + B \cdot Pos + C \cdot P \cdot r + D \cdot P \cdot Pos + E \cdot r + F \cdot r \cdot Pos + G \cdot P^2 + H \cdot Pos^2 + I \tag{20}$$

Where A=0.339830757; B=26.7091834; C=-0.589446283; D=0.342311309; E=-12.85820393; F=1.65152441; G=0.040712673; H=-2.105524434; I=-13.9490833126209 and where P is the relative pressure in the reactor in kPa; "Pos" is the position in the reactor (an integer dimensionless parameter between 1 and 8) and r is the H_2/CO molar ratio (also dimensionless).

Since the model shown in equation 20 is rather complicated, a 3D visual representation of the model is presented in figure 6 for a fixed position (Pos) value of 4. It can be interpreted from this figure that there is a very strong interaction between parameters. This model fits the data with a determination coefficient (R^2) superior to 0.93, which is quite high considering the methodology employed. While the R^2 coefficient gives a good indication of the relation between two series of data, it lacks in terms of information regarding the exactitude of a model. Therefore, other attributes such as the slope and the intercept of the predicted versus obtained measurement must be considered. Such information is available in figure 7 which illustrates the relationship between the model and the experimental data. In the present case, the slope equals to 1, and the intercept to 0, which indicates that the model fit the data fairly well.

[Figure 6 about here.]

[Figure 7 about here.]

It is tempting to conclude that the hydrophilic/hydrophobic "switch" could, in fact, be attributed to the regime where the reaction had taken place. Reaction occuring in the gas phase might encourage hydrophobic behavior of the coating, while coating growth onto the surface would tend to be hydrophilic. Another aspect that is to be looked into is if the reaction is adsorption limited or not, which is commonly observed for initiated-CVD (iCVD) polymers. A good way to verify this is by increasing temperature to see if the reaction rates improves. If not, it can be considered as adsorption limited. The effect of pressure mixed with a tight optimization of temperature profile in the reactor could tremendously improve the system's performance. While this study was a proof of concept of the feasibility of using PICVD, further investigation are obviously required in this regard.

It is still to early to determine if the reaction is a step growth or a chain growth. However the following hypothesis can be formulated, when there is the presence of an initiator as well as the presence of light, it is probable that the reaction is a chain polymerization one. UV light has been demonstrated to form free radical, which are the very core of a chain growth polymerization [24].

From a photopolymerization stand of view, it is usually accepted that those reactions requires a photo-initiator [25]. The present experiment have shown however that syngas was able to self-initiate in the presence of UV light, probably because of the formation of radicals. Experiments with H_2O_2 did promote the reaction by pushing the boundaries of contact angles measurements. The addition of hydrogen peroxide as a photoinitiator increased the range of water contact angles to 5° to 118°, and the angles seemed to be highly correlated with its flow rate. It is worth noticing that the total pressure is the dominant factor with this configuration. Generally, pressures slightly below 1 atm translates into hydrophilic surfaces, while pressures slightly higher than 1 atm resulted into hydrophobic surfaces. This could be interpreted as a transition between a kinetic controlled reaction to a mass transfer controlled reaction. As described in a

previous paper [4], a chemical vapor deposition reaction can occur either in the gas phase or on the surface of the substrates. If the kinetic rate is high, the reaction will occur in the gas phase, and the resulting compound will tend to deposit on any solid surfaces present in their pathway. To get in this regime, either high temperatures or high pressures must be reached. The second way of proceeding is through adsorption on the surface, promoted at lower pressures.

4.2. Characterization

GCMS. Samples of the outlet gas were analyzed by GCMS. The deposited compound has been identified as a close match to the bis(2-ethylhexyl)-phtalate. A sample GCMS spectrum is shown in figure 8. This characterization of species in the gas phase provides information on 2 fronts. First, it gives insight into the reactions taking place in the reactor - the molecule formed in rich in double-bonds and aromatics, and can have a relatively long chain length. Second, it provides information with respect to secondary products formed, which is key for eventual scale-up.

[Figure 8 about here.]

FTIR. The FT-IR was operated in attenuated total reflectance mode (ATR) in order to characterize the species present on the surface. With the available database, the closest match was phenol formaldehyde resin. Interestingly, the coating shared some properties with this family of resins, like its resistance to dissolution in solvents and its susceptibility to strong bases. That is the reason why NaOH was used for tube cleaning steps. While the match was not perfect, this indicates at least that the coated molecule is highly crosslinked and has a high concentration of C=C bonds. A sample FTIR spectrum resulting of a spectrum substraction with the one of the copper untreated is shown in figure 9, and its interpretation is given in table 4.

[Figure 9 about here.]

[Table 4 about here.]

4.3. FESEM

FESEM images helped to determine the general morphology of the sample's surface. Figure 10 shows the copper's surface before (left) and after (right) treatment. As one can see, the morphology of the surface clearly differs. The coated sample (on the right) consisted of tiny circular islands of approximately 40 nm of diameter. The fact that those islands appear as being white means that they are made of an electrically non-conductive material, which is consistent with the hypothesis of a polymer or a resin. It is expected that increased treatment time would lead to merging of these polymer islands on the surface.

[Figure 10 about here.]

4.4. Characterization based on properties

In order to confirm the possibility that the coating is made of a phenol formaldehyde-like resin, some further characterization has been performed based on basic properties.

Electrical resistivity:. Electrical resistivity was evaluated by the four point resistivity method at a voltage of 0.1 mV at a distance of 1 mm. The coated surface had an electrical resistivity 127 times higher than the copper alone for a thickness of about 1 micron roughly estimated by profilometry. Although the four point resistivity method is not a valid method to measure the exact resistivity coefficient of the material, it still give information about the insulating property of the coated material. Although this fact alone is inconclusive, it goes in favor of the hypothesis of phenol formaldehyde resin.

Solvability:. The coating was insoluble in common solvents (ex: acetone, methanol, ethanol, butanol, etc.) but could be remove using strong caustic (NaOH 5 M). Although this fact alone is inconclusive, it goes in favor of the hypothesis of phenol formaldehyde resin which is known to react with strong bases.

Visual inspection:. It is worth mentioning that the presence of red spots appeared in some cases and not in others. However, after investigation of the different parameters, this phenomenon was not significantly correlated to any of them. Those red spots tended to be superhydrophilic ($\leq 10°$) (see figure 11), more so than their transparent conterparts for the same experimental conditions. Over a hundred experiments have been conducted in order to find a pattern leading to such results. Despite the efforts, these red spots seemed to appear randomly and therefore, could not be statistically associated with any combination of known parameters. For the time being, figure 12 illustrates fairly well the appearance of these spots. Some variants appeared as shown in figure 5, where the red eventually evolved into a blueish color.

[Figure 11 about here.]

[Figure 12 about here.]

4.5. Hydrophobic recovery

Another concern that remains is the hydrophobic recovery, which consists of a hydrophilic surface that loses its property over time. During the experiment, it has been noticed that hydrophilic surfaces lose a great deal of their hydrophilicity over a short period of time (within 24 hours). For that reason, the water contact angles were measured in the hour following the deposition. According to Anderson and Ashurst hydrophobic recovery would be due to the migration of bulk material to the surface [26]. On the other hand, Wertheimer *et al.* affirm that hydrophobic recovery was due to hydrogen molecules which rotate inward caused by the attraction of hydrogen bond [27]. It has been observed that hydrophobic surfaces remained stable over time since no significant changes in measurement a week after was noticed.

5. Conclusion

The current process was able to produce both hydrophilic and hydrophobic coatings on copper surface. The feasability of using PICVD with simple gases such as H_2 and CO (syngas) for the functionalization of surfaces has been studied. In the tested conditions, it has been determined that syngas can be photopolymerized by UVC germicidal lamp to deposit functional groups onto copper. The deposited compound has been identified as being very similar to phenol formaldehyde resin. The gas sample analysis identified the bis(2-ethylhexyl)-phtalate as being produced in the reactor.

The current results seems to indicate that the potential of applications could be more numerous than originally planned. Also, the possibility to trigger a very specific water contact angle from a wide range between highly hydrophilic to highly hydrophobic opens up the possibilities even more. In other words, the wettability of a material can be tailored.

With a highly scalable method, it has been possible to produce high quality and dense coating in deposition temperature as low as room temperature and atmospheric or near-atmospheric pressures. While the effect of different process parameters remains to be optimized, the current results suggest that PICVD shows promises as a scalable and affordable technique for the functionalization of nanoparticles, as well as for any other surfaces. However, it is certain that more work has to be done to confirm the validity of PICVD for large scale applications. This technology being completely novel, experimental parameters, reactor design, as well as the scaling up are aspects that deserves to be investigated further.

A great start for future work would be to control more locally the temperature. In the case of this experiment, the substrate holder did not possess any cooling system and the whole reactor was assumed as being isothermal. It might have affected the deposition rate substantially. Precursor preheating might also help initiate the reaction. Since high deposition rate nor thickness is the objective for the purpose of surface functionalization, an enhancement of kinetic would rather translate into a decreased processing time. Other materials should be investigated as substrate in order to determine if the surface selection has an effect or not on the produced coating.

Also, the evaluation of the required concentration functional group on a surface that is necessary to have a positive effect onto the surface is another study that needs to be conducted. Finally, while the coating seemed very hard to remove from the surface, this study did not investigated the mechanical properties of the coating.

Acknowledgements

The authors would like to acknowledge the Fonds de recherche du Québec en nature et technologies (FRQNT), Natural Sciences and Engineering Research Council of Canada (NSERC), Sigma Xi Grants-in-Aid of Research, as well as the École Polytechnique de Montréal for their financial support. The authors

would also like to acknowledge the support of Centre for Characterization and Microscopy of Materials (CM^2) and the McGill University Plasma Processing Laboratory (PPL).

Bibliography

[1] J. Fendler, Nanoparticles and nanostructured films: preparation, characterization and applications, Wiley-Vch, 2008.
[2] Y. D. Dongshen Wen, Effective thermal conductivity of aqueous suspensions of carbon nanotubes (carbon nanotube nanofluids), Journal of thermophysics and heat transfer 18 (2004) 481–485.
[3] U. Kogelschatz, H. Esrom, J.-Y. Zhang, I. Boyd, High-intensity sources of incoherent uv and vuv excimer radiation for low-temperature materials processing, Applied Surface Science 168 (2000) 29 – 36.
[4] C. D. Dion, J. Tavares, Photo-initiated chemical vapor deposition as a scalable particle functionalization technology (a practical review), Powder Technology 239 (2013) 484 – 491.
[5] R. Sreenivasan, K. K. Gleason, Overview of strategies for the cvd of organic films and functional polymer layers, Chemical Vapor Deposition 15 (2009) 77–90.
[6] H. Yasuda, Plasma polymerization, Academic Press New York, 1985.
[7] K. Choy, Chemical vapour deposition of coatings, Progress in Materials Science 48 (2003) 57–170.
[8] S. H. Baxamusa, L. Montero, J. M. Dubach, H. A. Clark, S. Borros, K. K. Gleason, Protection of sensors for biological applications by photoinitiated chemical vapor deposition of hydrogel thin films, Biomacromolecules 9 (2008) 2857–2862.
[9] B. Zhang, Y.-C. Liao, S. Girshick, J. Roberts, Growth of coatings on nanoparticles by photoinduced chemical vapor deposition, Journal of Nanoparticle Research 10 (2008) 173–178.
[10] A. Tavasoli, A. Khodadadi, M. Mosavian, M. Abedinzadgan, A. Mohammadi, M. Azizi, A. Karimi, Photocatalytic enhancement of activity and selectivity of fischer-tropsch synthesis over cobalt based catalyst, in: 12th Oil, Gas and Petrochemical Congress.
[11] H. Okabe, Photochemistry of small molecules, Wiley New York, 1978.
[12] K. Scott, R. Willis, Atmospheric pollutants destroyed in an ultraviolet scrubber, Laboratory Practice 22 (1973) 103.
[13] C. von Sonntag, Free-radical-induced DNA damage and its repair: a chemical perspective, Springer, 2006.
[14] R. Young, G. Black, T. Slanger, Reaction and deactivation of o (d), The Journal of Chemical Physics 49 (1968) 4758.
[15] J. Friedrich, Mechanisms of plasma polymerization-reviewed from a chemical point of view, Plasma Processes and Polymers 8 (2011) 783–802.
[16] M. Trépanier, C. A. D. Dion, A. K. Dalai, N. Abatzoglou, Kinetics study on cnt-supported rukco fts catalyst in a fixed bed reactor, The Canadian Journal of Chemical Engineering 89 (2011) 1441–1450.
[17] C.-H. Zhang, Y. Yang, B.-T. Teng, T.-Z. Li, H.-Y. Zheng, H.-W. Xiang, Y.-W. Li, Study of an iron-manganese fischer–tropsch synthesis catalyst promoted with copper, Journal of Catalysis 237 (2006) 405–415.
[18] M. Julia, Free-radical cyclizations, Accounts of Chemical Research 4 (1971) 386–392.
[19] E. Andrzejewska, Photopolymerization kinetics of multifunctional monomers, Progress in Polymer Science 26 (2001) 605–665.
[20] G. Ozaydin-Ince, K. K. Gleason, Transition between kinetic and mass transfer regimes in the initiated chemical vapor deposition from ethylene glycol diacrylate, Journal of Vacuum Science & Technology A: Vacuum, Surfaces, and Films 27 (2009) 1135–1143.
[21] K. Goyal, R. Mahalingam, P. Pedrow, M. Osman, Mass transport characteristics in a pulsed plasma enhanced chemical vapor deposition reactor for thin polymer film deposition, Plasma Science, IEEE Transactions on 29 (2001) 42–50.
[22] H. S. Fogler, Elements of chemical reaction engineering (1999).
[23] J. Tavares, E. J. Swanson, S. Coulombe, Plasma Synthesis of Coated Metal Nanoparticles with Surface Properties Tailored for Dispersion, Plasma Processes and Polymers 5 (2008) 759–769.
[24] B. A. Jurkiewicz, G. R. Buettnerf, Epr detection of free radicals in uv-lrradiated skin: Mouse versus human, Photochemistry and photobiology 64 (1996) 918–922.
[25] T. Scherzer, Vuv-induced photopolymerization of acrylates, Macromolecular Chemistry and Physics 213 (2012) 324–334.
[26] A. Anderson, W. Ashurst, Enabling organosilicon chemistries on inert polymer surfaces with a vapor-deposited silica layer, Langmuir 25 (2009) 11541–11548.
[27] F. Truica-Marasescu, S. Guimond, P. Jedrzejowski, M. Wertheimer, Hydrophobic recovery of vuv/nh_3 modified polyolefin surfaces: Comparison with plasma treatments in nitrogen, Nuclear Instruments and Methods in Physics Research Section B: Beam Interactions with Materials and Atoms 236 (2005) 117–122.
[28] R. Silverstein, G. Bassler, T. Morrill, Spectrometric Identification of Organic Compounds, John Wiley & Sons, 4th edition edition, 1981.
[29] K. Nakanishi, P. H. Solomon, Infrared Absorption Spectroscopy, Holden-Day, 2nd edition edition, 1977.

List of Figures

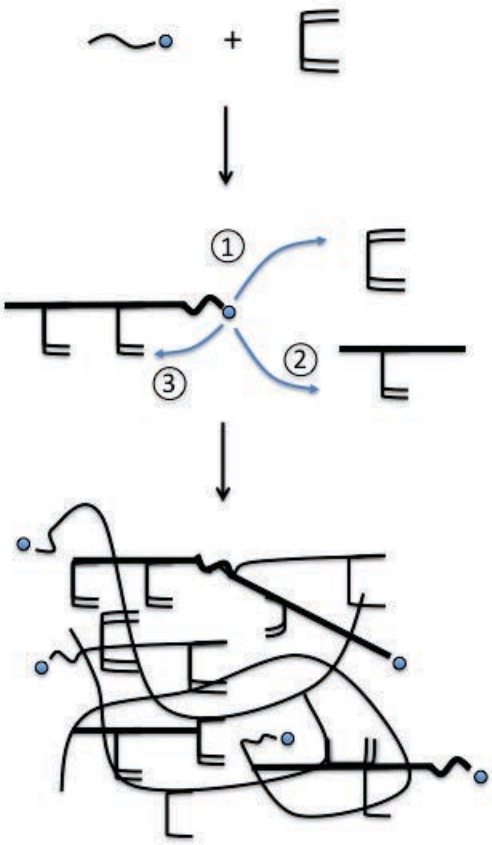

Figure 1: The formation of networks (reticulation), as described by Andrzejewska as combinations of three (3) propragation mechanisms that occur simultaneously. From the first to the second step, a radical group reacts with the monomer in various ways to form basic intermediates. From the second to the last step, an amalgam of reactions is taking place in order to create a random highly crosslinked network.

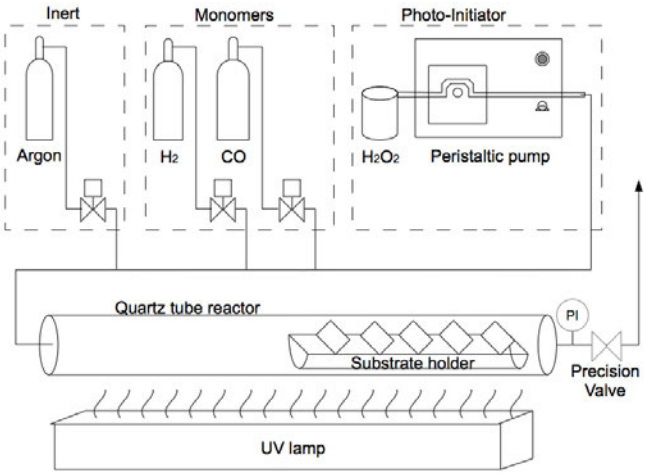

Figure 2: PICVD laboratory-scale setup used for the investigation

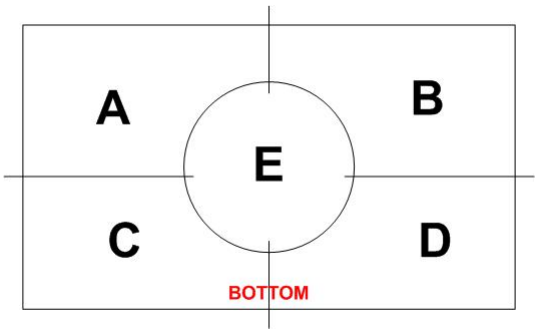

Figure 3: Mapping used for goniometry measurements

Figure 4: Top row: water contact angle of samples, respectively untreated, hydrophobic and hydrophilic. The picture underneath indicates the non-uniformity of the coating.

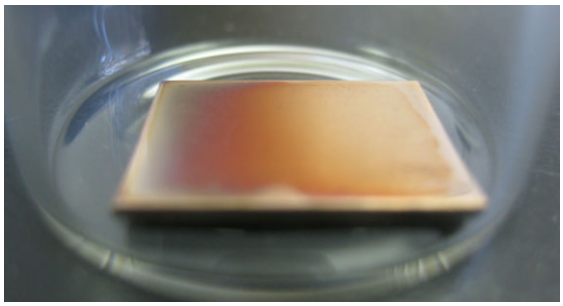

Figure 5: The red spot seem to cure into a blue color

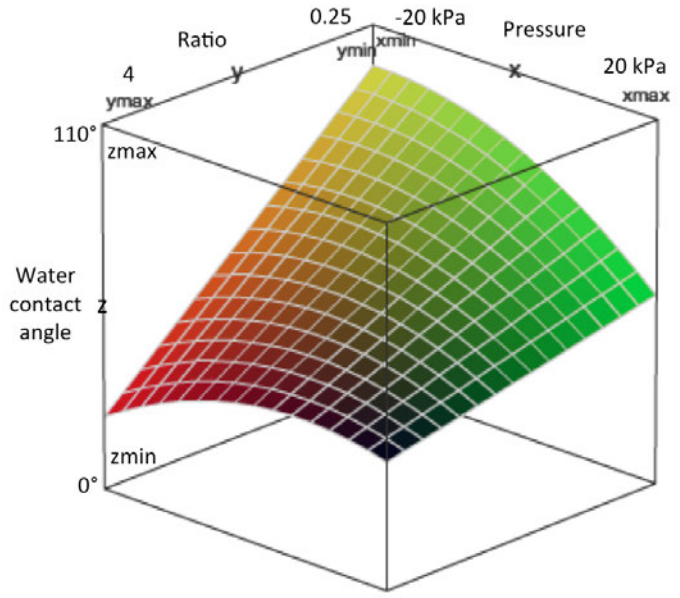

Figure 6: 3d representation of the empirical model where x axis represents the pressure in the reactor, y the gas ratio and z the water contact angle obtained for a fixed position value of 4 (Definition of the axes: x_{min}=-20 kPa; x_{max}=20 kPa; y_{min}=0.25; y_{max}=4; z_{min}=0°; z_{max}=110°.)

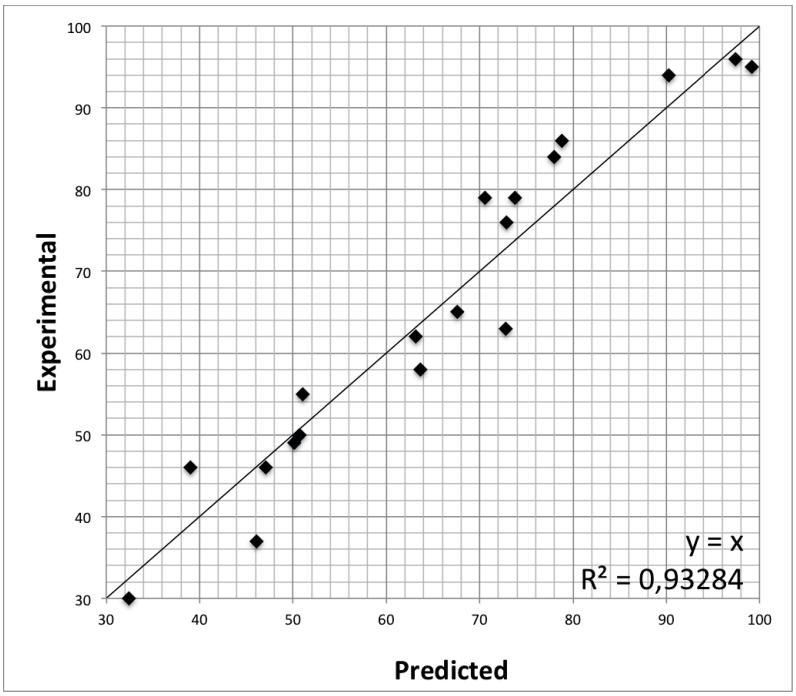

Figure 7: Experimental versus predicted for model shown in equation 20

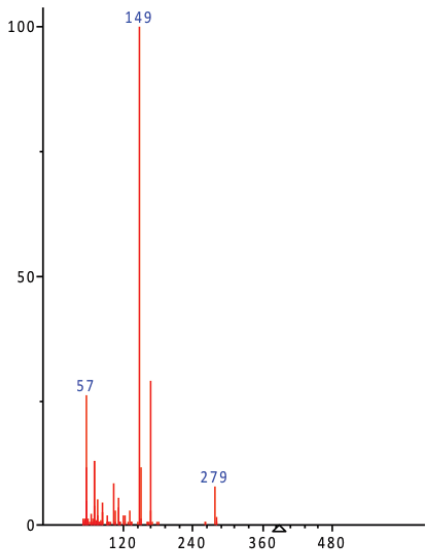

Figure 8: Mass spectrometry with peak retention time of 17.4 min

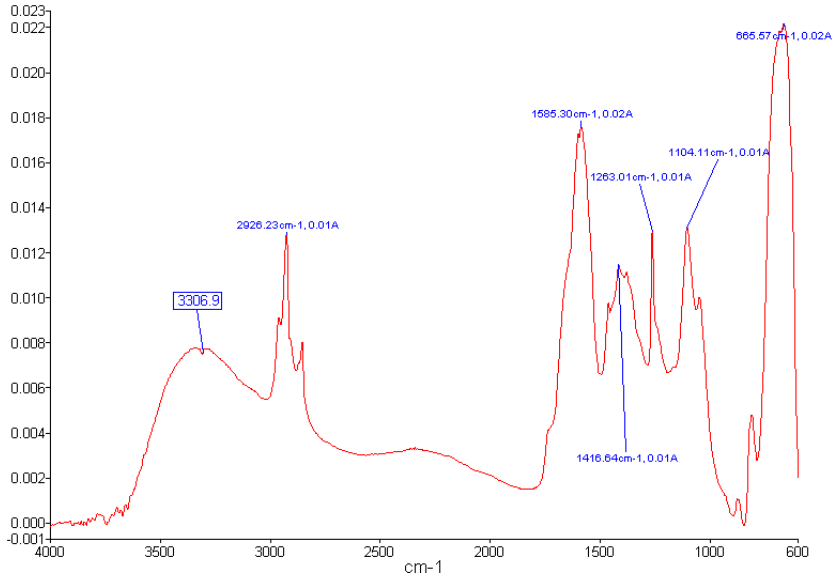

Figure 9: FTIR absorption spectrum (H_2/CO=2, P=0 kPa)

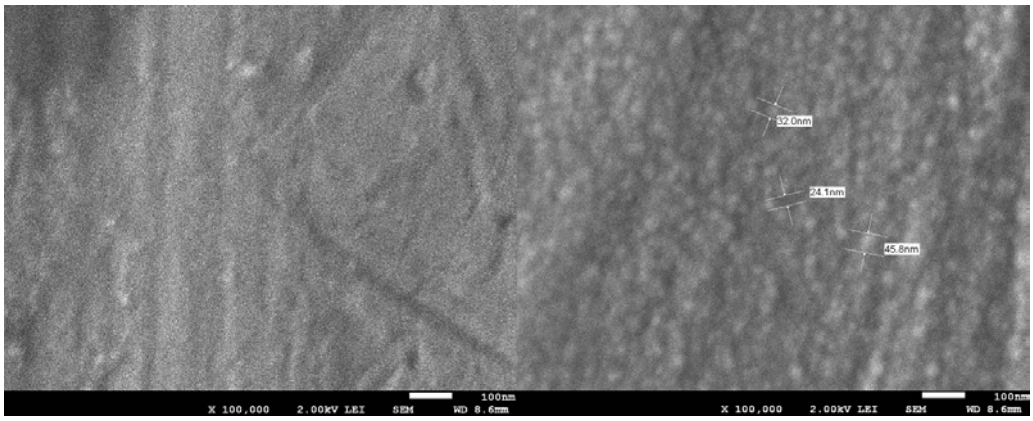

Figure 10: FESEM pictures of the surface before *(left)* and after *(right)* treatment

Figure 11: The spots exhibits very small contact angles

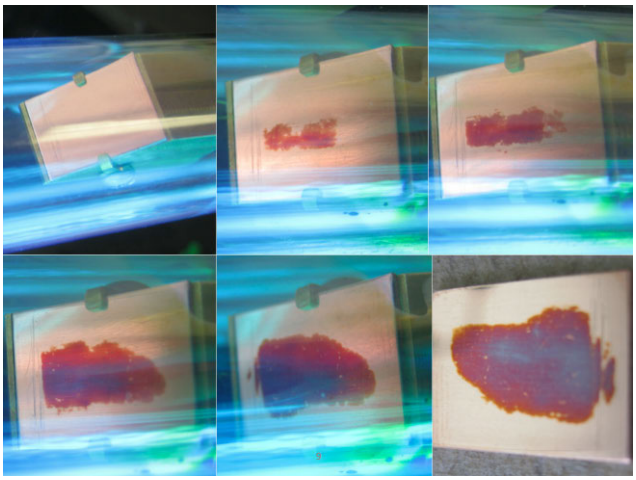

Figure 12: A growth progression of red spots over an hour

List of Tables

Table 1: Experimental data (1/3) - Experiments without H_2O_2

Process parameters				*Goniometry measurements*					*Basic Stats*			
P	**R**	**Pos**	**H_2O_2**	**A**	**B**	**C**	**D**	**E**	**Max**	**Min**	**Avg**	**Selected**
-10	0,125	4	0	62	37	42	67	67	67	37	55,0	37
-10	0,125	5	0	64	57	50	59	72	72	50	60,4	50
-10	0,125	6	0	63	57	55	71	71	71	55	63,4	55
-10	0,125	7	0	46	58	55	47	47	58	46	50,6	46
-10	0,125	8	0	71	46	72	72	72	72	46	66,6	46
10	4	4	0	47	46	45	64	30	64	30	46,4	30
10	4	5	0	49	49	52	52	54	54	49	51,2	49
10	4	6	0	72	66	66	58	76	76	58	67,6	58
10	4	7	0	68	74	76	68	68	76	68	70,8	76
10	4	8	0	67	63	70	84	84	84	63	73,6	84
-20	4	4	0	62	65	66	66	67	67	62	65,2	62
-20	4	5	0	76	79	79	79	79	79	76	78,4	79
-20	4	6	0	79	73	69	70	70	79	69	72,2	79
-20	4	7	0	68	67	64	63	73	73	63	67,0	63
-20	4	8	0	65	65	65	75	67	75	65	67,4	65
10	0,125	4	0	84	86	86	86	86	86	84	85,6	86
10	0,125	5	0	87	88	90	94	94	94	87	90,6	94
10	0,125	6	0	95	94	96	87	71	96	71	88,6	96
10	0,125	7	0	86	95	90	91	89	95	86	90,2	95
10	0,125	8	0	95	90	91	90	71	95	71	87,4	95

Table 2: Experimental data (2/3) - Experiments with H_2O_2

Process parameters				*Goniometry measurements*					*Basic Stats*			
P	**R**	**Pos**	**H_2O_2**	**A**	**B**	**C**	**D**	**E**	**Max**	**Min**	**Avg**	**Selected**
10	0,125	1	1	90	91	92	94	97	97	90	92,8	97
10	0,125	2	1	97	101	95	94	99	101	94	97,2	101
10	0,125	3	1	94	93	95	91	97	97	91	94,0	97
10	0,125	4	1	94	96	92	96	96	96	92	94,8	96
10	0,125	5	1	95	94	101	96	90	101	90	95,2	101
10	0,125	1	0,5	47	40	57	38	37	57	37	43,8	37
10	0,125	2	0,5	40	34	43	47	33	47	33	39,4	33
10	0,125	3	0,5	60	62	43	45	38	62	38	49,6	38
10	0,125	4	0,5	41	35	58	38	39	58	35	42,2	35
10	0,125	5	0,5	39	40	63	47	41	63	39	46	39
10	0,125	4	1	49	43	44	65	50	65	43	50,2	43
10	0,125	5	1	61	59	47	58	48	61	47	54,6	47
10	0,125	6	1	56	55	55	58	51	58	51	55,0	51
10	0,125	7	1	57	60	63	50	61	63	50	58,2	50
10	0,125	8	1	58	61	65	56	59	65	56	59,8	56
-15	0,125	1	1	62	62	60	33	62	62	33	55,8	33
-15	0,125	2	1	64	72	91	91	72	91	64	78,0	91
-15	0,125	3	1	58	50	47	44	45	58	44	48,8	44
-15	0,125	4	1	57	56	75	70	51	75	51	61,8	51
-15	0,125	5	1	68	72	67	69	65	72	65	68,2	65
-15	0,125	4	1	50	46	42	47	42	50	42	45,4	42

Table 3: Experimental data (2/3) - Experiments with H_2O_2

Process parameters				*Goniometry measurements*					*Basic Stats*			
P	**R**	**Pos**	**H_2O_2**	**A**	**B**	**C**	**D**	**E**	**Max**	**Min**	**Avg**	**Selected**
-15	0,125	5	1	41	50	55	55	49	55	41	50,0	41
-15	0,125	6	1	58	55	61	60	55	61	55	57,8	55
-15	0,125	7	1	62	62	62	64	63	64	62	62,6	62
-15	0,125	8	1	57	59	57	60	51	60	51	56,8	51
-15	0,125	1	0,5	62	54	47	45	52	62	45	52,0	45
-15	0,125	2	0,5	40	32	38	35	37	40	32	36,4	32
-15	0,125	3	0,5	37	42	40	51	50	51	37	44,0	37
-15	0,125	4	0,5	53	60	51	65	55	65	51	56,8	51
-15	0,125	5	0,5	90	82	85	81	81	90	81	83,8	90
-15	0,125	4	0,5	99	100	87	86	82	100	82	90,8	100
-15	0,125	5	0,5	58	46	50	52	60	60	46	53,2	46
-15	0,125	6	0,5	49	56	52	52	50	56	49	51,8	49
-15	0,125	7	0,5	55	56	59	52	55	59	52	55,4	52
-15	0,125	8	0,5	50	53	53	54	50	54	50	52,0	50
10	0,125	4	0,5	101	74	91	99	80	101	74	89,0	101
10	0,125	5	0,5	94	91	95	94	92	95	91	93,2	95
10	0,125	6	0,5	93	89	100	94	93	100	89	93,8	100
10	0,125	7	0,5	79	89	90	90	88	90	79	87,2	90
10	0,125	8	0,5	90	95	92	93	90	95	90	92	95

Table 4: FTIR table - Analysis of the spectrum shown in figure 9

Wavelength (cm^{-1}	**Bond**	**Additional information**	**References**
3300	O-H stretch	strong, broad (alcohol)	[28]
2925	C-H stretch	(Alkane)	[28]
1585	C=C aromatic stretch	medium-weak, multiple bands	[28]
1415	C=C aromatic stretch	medium-weak, multiple bands	[28]
1263	C-O-C stretch	(Ether)	[28]
1100	C-O stretch	(Alcohol)	[28]
666	O=C=O scissoring	Confirmed by the bumb around 2350 cm^{-1}	[29]